Title
DISCRETE ANALYSIS OF STOCHASTIC NMR - I

Authors
Wong, S.T.S.
Roos, M.S.
Newmark, R.D.

Publication Date
1989-03-01

LBL-27008
Preprint

Lawrence Berkeley Laboratory
UNIVERSITY OF CALIFORNIA

Submitted to Journal of Magnetic Resonance

Discrete Analysis of Stochastic NMR – I

S.T.S. Wong, M.S. Roos, R.D. Newmark, and T.F. Budinger

March 1989

Donner Laboratory

Biology & Medicine Division

Prepared for the U.S. Department of Energy under Contract Number DE-AC03-76SF00098.

DISCLAIMER

Discrete Analysis of Stochastic NMR – I

S.T.S. Wong, M.S. Roos, R.D. Newmark and T.F. Budinger

Donner Laboratory, Lawrence Berkeley Laboratory, University of California,

Berkeley, CA 94720

Sam T. S. Wong

Department of Radiology

Brigham and Women's Hospital

Harvard Medical School

75 Francis St.

Boston, MA 02115

Abstract

Stochastic NMR is an efficient technique for high field *in vivo* imaging and spectroscopic studies where the peak RF power required may be prohibitively high for conventional pulsed NMR techniques. This paper presents a theoretical analysis of a stochastic NMR spectroscopy experiment that consists of exciting the spin system with RF pulses where the flip angles or the phases of the pulses are samples of a discrete stochastic process. The experiment is formulated as a stochastic difference equation which is then converted to ordinary deterministic difference equations describing the input-output cross-correlation, average signal power and signal power spectrum. The solutions of these equations are used to study spectral distortions as the spin system is saturated with a high power excitation, to obtain an optimum excitation power level that gives the maximum signal-to-noise ratio and to evaluate the contribution of systematic noise to the overall signal-to-noise ratio of the experiment. The specific case of random flip angle excitation is analyzed. Results show that high power excitation may cause line broadening, a notch artifact and non-uniform response across the spectrum. Experimental results are also presented to show that the discrete analysis provides an accurate description of practical experiments.

Introduction

In a conventional pulsed FT-NMR experiment, a short (1 to 100 μsec) RF pulse is usually repeated at intervals comparable to the longitudinal relaxation time constant T_1 (typically 10^{-2} to 10^2 seconds). This corresponds to a very small duty cycle for the RF amplifier. The power needed for an NMR experiment is determined by the excitation bandwidth, which is proportional to the range of chemical shift in the sample, which in turn is proportional to the magnetic field. The excitation bandwidth also determines the duration of the RF pulse in pulsed FT-NMR. For a given range of chemical shift, an increase in the static field strength corresponds to a decrease in pulse duration. This implies that the peak RF power must be increased in order to deliver the same amount of RF energy to the sample. It may be difficult or unsafe to attain the necessary power in experiments with large conducting samples at high field. For example, a 20μsec RF pulse for ^{13}C spectroscopy of the human head in a 4.7 Tesla static field requires a peak power of approximately 400KW.

In 1966, the same year that he introduced FT-NMR, Ernst (*1*) also introduced the use of noise-like RF excitation. Experiments that involve noise-like RF excitation are a sub-class of what we will call stochastic NMR. The noise-like RF delivers the excitation energy more evenly in time than conventional pulsed FT-NMR, resulting in a reduction of the peak RF power requirement by several orders of magnitude. This makes stochastic NMR an efficient technique for high field *in vivo* imaging and spectroscopic studies where the peak RF power required may be prohibitively high for conventional pulsed NMR techniques.

The impulse response of an unknown linear system is given by the cross-correlation of the input and output of the system when the system is excited by zero mean Gaussian white noise (Fig. 1a). Ernst (*2*) and Kaiser (*5*) applied this principle to stochastic NMR independently in 1970. The NMR spin system was excited by a stochastic RF signal. The first order input-output cross-correlation was used to approximate the Free Induction Decay (FID) obtained by a conventional

pulsed FT-NMR experiment (Fig. 1b). The Fourier transform of the cross-correlation was shown to be an estimate of the spectrum. Ernst showed that stochastic NMR not only eases some of the difficulties in instrument design, but also provides a controllable resolution and a sensitivity similar to those of conventional pulsed FT-NMR. Ziessow (*3*, *4*) and Kaiser (*7*) have shown that with binary maximum length sequence (MLS) excitations, the input-output cross-correlation could be processed by Hadamard transforms which required no multiplication, and hence is even faster than the FFT. In addition, the periodicity of the binary MLS allowed coherent signal averaging to be used to improve the S/N ratio. Blumich and Ziessow (*6*) and Kaiser and Knight (*8*,*9*) have shown that the data obtained with stochastic excitation can also be used to obtain multi-dimensional spectroscopic data. This was demonstrated experimentally by Blümich and Ziessow (*10-16*).

So far, all the analyses of the stochastic experiment have assumed continuous random excitation (*1-5*, *8-9*, *17*). Continuous random excitation is undesirable from a practical experimental point of view since the RF transmitter is usually gated off during data sampling in order to avoid saturation of the receiver. The discrete stochastic experiment, shown in Fig. 2 is more practical: A stochastic sequence of RF excitations, $\alpha(n)$, is applied at intervals of T_R seconds and one data point is sampled after every RF pulse. The theoretical analysis based on continuous excitation is at best an approximate description of this experiment. It is the aim of this paper to characterize the discrete stochastic experiment, obtaining analytic results that correspond exactly to experiments as they are implemented.

The driven NMR spin system is intrinsically nonlinear. The magnetization response is a nonlinear function of the RF excitation. The FID that results from a single one pulse excitation is proportional to the linear component of the nonlinear magnetization response. When a sequence of pulses are applied, the response after the second pulse will no longer be a pure FID. This is why pulsed FT-NMR requires a considerable time delay after data sampling before the next RF

pulse is applied. In stochastic NMR, RF pulses with low power are applied in rapid succession. The spin system can easily be pushed towards the nonlinear regime. The first order input-output cross-correlation shown in Fig. 1b will not always give the FID. The objective of this paper is to understand the performance of the discrete stochastic NMR spectroscopy experiment by analyzing the following aspects of the experiment: (1) The conditions under which the first order input-output cross-correlation will be a faithful estimate of the FID obtained by a conventional pulsed FT-NMR experiment, (2) the saturation behavior when the excitation power is high, (3) the experimental parameters that maximize the S/N ratio, and (4) evaluation of the signal power spectrum as an alternative estimate of the real spectrum.

In all previous analyses, the RF vector was assumed to lie along one axis in the rotating frame with the flip angle being random. This type of excitation will be denoted as random flip angle excitation. The analysis in a later section of this work will show that this type of excitation causes undesirable spectral distortions as the RF excitation power is increased. This result will be used to explain discrepancies and artifacts in earlier results (*9*,*17*). A subsequent paper (Part II (*18*)) will analyze two new types of random RF excitations that do not exhibit such artifacts. One type will be denoted as random phase excitation wherein the RF pulses have the same flip angles but the phase of the RF vector is random. The other type is denoted as random quadrature excitation where the RF vector consists of two orthogonal components that are statistically uncorrelated but have identical probability distributions.

So far, binary random sequences and discrete Gaussian white noise are the two most favorable stochastic sequences to be employed in stochastic NMR experiment. Binary random excitation is popular because it can be approximated by pseudo-random binary MLS, it is easy to implement in hardware (*19*) and it allows the Hadamard transform to be used to speed up the calculation

of cross-correlations. Gaussian white noise has statistical properties that simplify the theoretical analysis tremendously. This paper will show that the performance of these two types of stochastic sequences is very similar.

It is assumed throughout this work that the spin system consists of isolated spin 1/2 nuclei, so that the Bloch equations are applicable. The duration of each RF pulse is assumed to be short compared to the relaxation time constants, T_1 and T_2. This assumption allows the effects of each RF pulse to be represented by the multiplication of the magnetization vector with a rotation matrix. The RF pulses are also assumed to be sufficiently short that off resonance dephasing of the magnetization is insignificant during the RF pulses.

Derivation of explicit expressions describing the stochastic response and reconstructed spectra is facilitated by the assumptions that the excitation sequences are wide-sense stationary and that NMR spin system is stationary. A stationary spin system in this context means that the spins do not experience a change in spin characteristics, e.g. T_1, T_2 and resonance offset, during the experiment. Such a change of characteristics might be caused by macroscopic motion of the sample in the presence of a magnetic field gradient, application of a time varying gradient or a fluctuation in the static magnetic field. A stochastic sequence $x(n)$ is said to be wide-sense stationary if it possesses finite second moments and its auto-correlation $\langle x(n)x^*(m)\rangle$ is a function only of the absolute difference $|n-m|$. A variety of algorithms are available to generate pseudo-random sequences that are wide-sense stationary (*20*).

A third assumption, required for data reconstruction, is ergodicity. Calculations of the input-output cross-correlation, average signal power and signal power spectrum all involve taking the expectation of stochastic sequences. The expectation can be obtained by ensemble averaging. In terms of the stochastic NMR experiment, this means repeating the experiment many times and

taking the average of the results from each run. However, there is a waiting period at the beginning of the experiment for the average magnetization to acquire a steady state. The data collected in this period cannot be used in the reconstruction. This loss of experiment time can be avoided if the ensemble average is replaced by a time average. For example, the auto-correlation of the stochastic process $x(n)$ is approximated by a finite sum over the time index n:

$$\langle x(n)\, x^*(n-m)\rangle \approx \frac{1}{N}\sum_{n=0}^{N-1} x(n)\, x^*(n-m), \qquad [1]$$

where the symbol * is the complex conjugate operator. The process $x(n)$ is said to be ergodic if the approximation becomes an equality when N approaches infinity. Unfortunately, it is very difficult to show that a process is ergodic. However, computer simulated and experimental results for the stochastic NMR experiments with wide-sense stationary excitations using time averaging show excellent agreement with theory based on expectation. This implies that the ergodic assumption is not totally unjustified. The choice of N will be discussed in Part II (*18*).

Discrete Formulation for Generalized Excitations

This section will provide an analysis for a generalized stochastic RF excitation. The results of the generalized analysis will be made specific in the next section for the case of random flip angle excitation. The approach taken for the analysis is shown as a block diagram in Fig. 3. In the block diagram $M(n) = [M_x(n), M_y(n), M_z(n)]^T$ is the magnetization vector immediately after the n^{th} RF pulse. The complex quantity $M_{xy}(n) = M_x(n) + i\, M_y(n)$ is the transverse magnetization. Quadrature detection gives a signal proportional to $M_{xy}(n)$. From the Bloch equation, a stochastic difference equation describing the pulse-to-pulse behavior of $M(n)$ is derived. Instead of solving this stochastic difference equation, it is combined with the excitation sequence $\alpha(n)$ to give a deterministic difference equation describing the cross-correlation of $M(n)$ and $\alpha(n)$, which can then be solved to obtain the input-output cross-correlation. The Fourier transform of the cross-correlation gives an estimate of the spectrum. The estimate can be used to study the saturation

effects as the excitation power is increased.

From the stochastic difference equation an equation of the covariance matrix of $M(n)$ can be obtained. This equation is a set of six simultaneous equations with six unknowns which are the variances and covariances of $M_x(n)$, $M_y(n)$ and $M_z(n)$. The average signal power is the sum of the variances of $M_x(n)$ and $M_y(n)$. A plot of the average signal power as a function of the excitation power will show the excitation power level that gives the maximum S/N ratio. The stochastic difference equation can also be turned into a difference equation for the auto-correlation matrix of the magnetization vector $M(n)$. The sum of the first two diagonal elements of the auto-correlation matrix is the auto-correlation of the transverse magnetization. The Fourier transform of this sum gives the signal power spectrum.

Consider the stochastic experiment depicted in Fig. 2 where the sample is excited by an RF pulse every T_R seconds and one signal data point is sampled right after the pulse. With the assumption of isolated spins the analysis need concentrate on only one spin species with relaxation parameters T_1 and T_2 and equilibrium magnetization M_e. Assume that the RF vector lies only in the transverse plane and is proportional to the excitation sequence $\boldsymbol{\alpha}(n) = [\alpha_x(n),\ \alpha_y(n),\ 0]^T$. Without loss of generality, $\boldsymbol{\alpha}(n)$ will be regarded as the RF vector. The average power of $\boldsymbol{\alpha}(n)$ will be treated as the average RF power. Furthermore, $\boldsymbol{\alpha}(n)$ is assumed to be an ergodic and wide-sense stationary stochastic sequence with mean $\boldsymbol{\mu}_\alpha = [\mu_x, \mu_y, 0]^T$ and auto-covariance

$$\langle [\boldsymbol{\alpha}(n) - \boldsymbol{\mu}_\alpha]\,[\boldsymbol{\alpha}(m) - \boldsymbol{\mu}_\alpha]^T \rangle = C_\alpha\, \delta_{nm}, \qquad [2]$$

where C_α is the covariance matrix of $\boldsymbol{\alpha}(n)$ and δ_{nm} is the Kronecker delta function. The trace of C_α is the average random excitation power and is denoted as

$$\alpha^2 = \langle (\alpha_x(n) - \mu_x)^2 + (\alpha_y(n) - \mu_y)^2 \rangle. \qquad [3]$$

With the right choice of constant of proportionality α can be regarded as the root mean square (RMS) flip angle and is expressed in radians in all the calculations. However, it is usually referred

to in this paper in degrees.

Assuming that the RF pulse duration is short compared with the relaxation time constants T_1 and T_2, the Bloch equations can be solved for the magnetization vector as it varies from one RF pulse to the next. The effects of the n^{th} RF pulse can be summarized by a rotation matrix $\boldsymbol{R}_\alpha(n)$ which is a function of $\alpha(n)$. Denote the amount of interpulse dephase of the transverse magnetization as θ. It is a function of factors such as resonance offset, chemical shift, field inhomogeneities or applied magnetic field gradients. For the rest of this analysis assume that resonance offset is the only source of interpulse dephase. For a spin ν Hz above resonance, θ is given by

$$\theta = 2\pi\nu T_R \qquad [4]$$

and the effect of the interpulse dephase is summarized by the matrix

$$\boldsymbol{R}_\theta = \begin{bmatrix} E_2\cos\theta & E_2\sin\theta & 0 \\ -E_2\sin\theta & E_2\cos\theta & 0 \\ 0 & 0 & E_1 \end{bmatrix},$$

where $E_1 = e^{-T_R/T_1}$ and $E_2 = e^{-T_R/T_2}$. The pulse-to-pulse trajectory of the magnetization vector is described by the following stochastic vector difference equation

$$\boldsymbol{M}(n) = \boldsymbol{R}_\alpha(n)\,[\boldsymbol{R}_\theta\,\boldsymbol{M}(n-1) + \boldsymbol{C}], \qquad [5]$$

where $\boldsymbol{C}$ is a constant vector given by

$$\boldsymbol{C} = \begin{bmatrix} 0 \\ 0 \\ M_e(1-E_1) \end{bmatrix} \qquad [6]$$

and M_e is the equilibrium magnetization of the sample in the static main field.

The matrix $\boldsymbol{R}_\theta$ has eigenvalues with magnitudes smaller than one. This fact together with Eq. [2] imply that the mean $\langle \boldsymbol{M}(n) \rangle$ and the covariance $\langle \boldsymbol{M}(n)\,\boldsymbol{M}^T(n) \rangle$ will approach steady state

values for large enough n, and the magnetization vector $\boldsymbol{M}(n)$ becomes a wide-sense stationary stochastic sequence. In addition, Eqs. [2] and [5] imply that $\boldsymbol{R}_\alpha(n)$ and $\boldsymbol{M}(m)$ are uncorrelated for all m less than n. Taking the expectation of both sides of Eq. 5 and rearranging terms gives

$$\boldsymbol{\mu}_M = (\boldsymbol{I} - \boldsymbol{\mu}_R \boldsymbol{R}_\theta)^{-1} \boldsymbol{\mu}_R \boldsymbol{C}, \qquad [7]$$

where $\boldsymbol{\mu}_M = \langle \boldsymbol{M}(n) \rangle$, $\boldsymbol{\mu}_R = \langle \boldsymbol{R}_\alpha(n) \rangle$ and I is the 3x3 identity matrix.

The first order input-output cross-covariance $k_1(m)$ is an estimate of the FID. It is defined as the cross-covariance of the complex input $\alpha_{xy}(n) = [\alpha_x(n) + i\,\alpha_y(n)]$ with the complex transverse magnetization $M_{xy}(n)$

$$\begin{aligned} k_1(m) &= \frac{1}{\alpha^2} \langle (M_{xy}(n) - \langle M_{xy}(n) \rangle) (\alpha_{xy}(n-m) - \langle \alpha_{xy}(n-m) \rangle)^* \rangle \\ &= \frac{1}{\alpha^2} \boldsymbol{B}^\dagger [\langle \boldsymbol{M}(n)\, \boldsymbol{\alpha}^T(n-m) \rangle - \boldsymbol{\mu}_M\, \boldsymbol{\mu}_\alpha^T]\, \boldsymbol{B}, \end{aligned} \qquad [8]$$

where $\boldsymbol{B} = [1,\ -i,\ 0]^T$ and the superscript † is the complex conjugate transpose operator. $k_1(m)$ is independent of n because both the input and the output sequences are wide-sense stationary. When m is less than zero, $\boldsymbol{\alpha}(n-m)$ and $\boldsymbol{M}(n)$ are uncorrelated and so $\langle \boldsymbol{M}(n)\, \boldsymbol{\alpha}^T(n-m) \rangle = \langle \boldsymbol{M}(n) \rangle \langle \boldsymbol{\alpha}(n-m) \rangle^T$, i.e., $k_1(m) = 0$. This is expected since the spin system is a causal system. For m larger than zero, Eq. [5] gives

$$\begin{aligned} &\langle \boldsymbol{M}(n)\, \boldsymbol{\alpha}^T(n-m) \rangle - \boldsymbol{\mu}_M\, \boldsymbol{\mu}_\alpha^T \\ &= \boldsymbol{\mu}_R \boldsymbol{R}_\theta [\langle \boldsymbol{M}(n-1)\, \boldsymbol{\alpha}^T(n-m) \rangle - \boldsymbol{\mu}_M\, \boldsymbol{\mu}_\alpha^T] \\ &= \boldsymbol{\mu}_R \boldsymbol{R}_\theta [\langle \boldsymbol{M}(n-1)\, \boldsymbol{\alpha}^T((n-1) - (m-1)) \rangle - \boldsymbol{\mu}_M\, \boldsymbol{\mu}_\alpha^T] \\ &= \boldsymbol{\mu}_R \boldsymbol{R}_\theta [\langle \boldsymbol{M}(n)\, \boldsymbol{\alpha}^T(n - (m-1)) \rangle - \boldsymbol{\mu}_M\, \boldsymbol{\mu}_\alpha^T], \end{aligned} \qquad [9]$$

where the fact that $\langle \boldsymbol{M}(n)\, \boldsymbol{\alpha}^T(n-m) \rangle$ is wide-sense stationary has been used. This is now an ordinary deterministic difference equation for $\langle \boldsymbol{M}(n)\, \boldsymbol{\alpha}^T(n-m) \rangle - \boldsymbol{\mu}_M\, \boldsymbol{\mu}_\alpha^T$ with index m. The solution is

$$\langle \boldsymbol{M}(n)\, \boldsymbol{\alpha}^T(n-m) \rangle - \boldsymbol{\mu}_M\, \boldsymbol{\mu}_\alpha^T = (\boldsymbol{\mu}_R \boldsymbol{R}_\theta)^m [\langle \boldsymbol{M}(n)\, \boldsymbol{\alpha}^T(n) \rangle - \boldsymbol{\mu}_M\, \boldsymbol{\mu}_\alpha^T]. \qquad [10]$$

Combining Eqs. [8] and [10] gives

$$k_1(m) = \frac{1}{\alpha^2}\, \boldsymbol{B}^\dagger\, (\boldsymbol{\mu}_R\, \boldsymbol{R}_\theta)^m\, \boldsymbol{A}\, \boldsymbol{B}, \qquad [11]$$

where

$$\boldsymbol{A} = \langle \boldsymbol{M}(n)\, \boldsymbol{\alpha}^T(n) \rangle - \boldsymbol{\mu}_M\, \boldsymbol{\mu}_\alpha^T. \qquad [12]$$

The $\mathcal{Z}$-transform of $k_1(m)$ is defined as

$$\mathcal{Z}\{k_1\}(z) = \sum_{m=0}^{\infty} k_1(m)\, z^{-m}. \qquad [13]$$

The summation is not performed over negative m since $k_1(m)$ is zero for negative m. The product $\boldsymbol{R}_\alpha(n)\, \boldsymbol{R}_\theta$ represents rotations and relaxation of the magnetization vector so its eigenvalues are less than one and $(\boldsymbol{\mu}_R\, \boldsymbol{R}_\theta)^m$ approaches zero as m approaches infinity. Substituting $k_1(m)$ from Eq. [11] into Eq. [13], the $\mathcal{Z}$-transform of $k_1(m)$ is given by

$$\begin{aligned} \mathcal{Z}\{k_1\}(z) &= \frac{1}{\alpha^2} \boldsymbol{B}^\dagger \sum_{m=0}^{\infty} (\boldsymbol{\mu}_R \boldsymbol{R}_\theta)^m\, z^{-m}\, \boldsymbol{A}\, \boldsymbol{B} \\ &= \frac{1}{\alpha^2} \boldsymbol{B}^\dagger\, (\boldsymbol{I} - \boldsymbol{\mu}_R\, \boldsymbol{R}_\theta\, z^{-1})^{-1}\, \boldsymbol{A}\, \boldsymbol{B}. \end{aligned} \qquad [14]$$

An estimate of the spectrum is given by the inverse Fourier transform of $k_1(m)$, which can be obtained by evaluating the $\mathcal{Z}$-transform of $k_1(m)$ on the unit circle of the complex $\mathcal{Z}$-plane:

$$\begin{aligned} K_1(\omega) &= \mathcal{Z}\{k_1\}(e^{-i\omega T_R}) \\ &= \frac{1}{\alpha^2} \boldsymbol{B}^\dagger\, (\boldsymbol{I} - \boldsymbol{\mu}_R\, \boldsymbol{R}_\theta\, e^{i\omega T_R})^{-1}\, \boldsymbol{A}\, \boldsymbol{B}. \end{aligned} \qquad [15]$$

This is a description of the reconstructed spectrum for a general excitation sequence $\boldsymbol{\alpha}(n)$.

The average signal power is defined as

$$\begin{aligned} P &= \langle M_x^2(n) + M_y^2(n) \rangle \\ &= \boldsymbol{B}^\dagger\, \langle \boldsymbol{M}(n)\, \boldsymbol{M}^T(n) \rangle\, \boldsymbol{B} \\ &= \boldsymbol{B}^\dagger\, \langle \boldsymbol{M}\, \boldsymbol{M}^T \rangle\, \boldsymbol{B}. \end{aligned} \qquad [16]$$

The signal correlation matrix, $\langle M\, M^T\rangle$, is independent of n because $M(n)$ is wide-sense stationary. From Eq. [5] $\langle M\, M^T\rangle$ is given by the solution of the matrix equation

$$\begin{aligned}\langle M\, M^T\rangle &= \langle R_\alpha(n)\, R_\theta\, \langle M\, M^T\rangle\, R_\theta^T\, R_\alpha^T(n)\rangle + \langle R_\alpha(n)\, R_\theta\, \mu_M\, C^T\, R_\alpha^T(n)\rangle \\ &\quad + \langle R_\alpha(n)\, C\, \mu_M^T\, R_\theta^T\, R_\alpha^T(n)\rangle + \langle R_\alpha(n)\, C\, C^T\, R_\alpha^T(n)\rangle, \end{aligned} \quad [17]$$

which is a set of six simultaneous equations with six unknowns.

The covariance of the complex signal M_{xy} is defined as

$$\begin{aligned} r(m) &= \langle [M_{xy}(n) - \langle M_{xy}(n)\rangle]\, [M_{xy}(n-m) - \langle M_{xy}(n-m)\rangle]^*\rangle \\ &= B^\dagger\, [\langle M(n)\, M^T(n-m)\rangle - \mu_M\, \mu_M^T]\, B. \end{aligned} \quad [18]$$

For $m \geq 0$, multiplying both sides of equation Eq. [5] with $M^T(n-m)$, taking the expectation and then subtracting $\mu_M\, \mu_M^T$ gives

$$\begin{aligned} &\langle M(n) M^T(n-m)\rangle - \mu_M\, \mu_M^T \\ &= \mu_R\, R_\theta\, [\langle M(n-1)\, M^T(n-m)\rangle - \mu_M\, \mu_\alpha^T] \\ &= \mu_R\, R_\theta\, [\langle M(n-1)\, M^T((n-1)-(m-1))\rangle - \mu_M\, \mu_\alpha^T] \\ &= \mu_R\, R_\theta\, [\langle M(n)\, M^T(n-(m-1))\rangle - \mu_M\, \mu_\alpha^T]. \end{aligned} \quad [19]$$

Once again, an ordinary deterministic difference equation is obtained. The solution is

$$\langle M(n) M^T(n-m)\rangle - \mu_M\, \mu_M^T = (\mu_R\, R_\theta)^m\, [\langle M\, M^T\rangle - \mu_M\, \mu_M^T]. \quad [20]$$

Similarly, for $m \leq 0$,

$$\langle M(n) M^T(n-m)\rangle - \mu_M\, \mu_M^T = [\langle M\, M^T\rangle - \mu_M\, \mu_M^T]\, (\mu_R^T\, R_\theta^T)^{-m}. \quad [21]$$

The $\mathcal{Z}$-transform of $r(m)$ is then given by

$$\mathcal{Z}\{r\}(z) = \sum_{m=-\infty}^{\infty} r(m)\, z^{-m}$$

$$
\begin{aligned}
&= \boldsymbol{B}^{\dagger}\left[(\boldsymbol{I}-\boldsymbol{\mu}_R\,\boldsymbol{R}_\theta\,z^{-1})^{-1}\left(\langle \boldsymbol{M}\,\boldsymbol{M}^T\rangle-\boldsymbol{\mu}_M\,\boldsymbol{\mu}_M^T\right)\right.\\
&\quad +(\langle \boldsymbol{M}\,\boldsymbol{M}^T\rangle-\boldsymbol{\mu}_M\,\boldsymbol{\mu}_M^T)\,(\boldsymbol{I}-\boldsymbol{\mu}_R^T\,\boldsymbol{R}_\theta^T\,z)^{-1}\\
&\quad \left.-(\langle \boldsymbol{M}\,\boldsymbol{M}^T\rangle-\boldsymbol{\mu}_M\,\boldsymbol{\mu}_M^T)\right]\boldsymbol{B}. \qquad [22]
\end{aligned}
$$

The power spectrum is the $\mathcal{Z}$-transform of $r(m)$ evaluated on the unit circle of the complex $\mathcal{Z}$-plane:

$$
\begin{aligned}
S(\omega) &= \mathcal{Z}\{r\}(e^{-i\omega T_R})\\
&= \boldsymbol{B}^{\dagger}\left[(\boldsymbol{I}-\boldsymbol{\mu}_R\,\boldsymbol{R}_\theta\,e^{i\omega T_R})^{-1}\left(\langle \boldsymbol{M}\,\boldsymbol{M}^T\rangle-\boldsymbol{\mu}_M\,\boldsymbol{\mu}_M^T\right)\right.\\
&\quad +(\langle \boldsymbol{M}\,\boldsymbol{M}^T\rangle-\boldsymbol{\mu}_M\,\boldsymbol{\mu}_M^T)\,(\boldsymbol{I}-\boldsymbol{\mu}_R^T\,\boldsymbol{R}_\theta^T\,e^{-i\omega T_R})^{-1}\\
&\quad \left.-(\langle \boldsymbol{M}\,\boldsymbol{M}^T\rangle-\boldsymbol{\mu}_M\,\boldsymbol{\mu}_M^T)\right]\boldsymbol{B}. \qquad [23]
\end{aligned}
$$

Random Flip Angle Excitation

In this section, it is assumed, without loss of generality, that the RF excitation vector lies only along the x-axis of the rotating frame. The excitation vector $\boldsymbol{\alpha}(n)$ has only one non-zero component, $\alpha_x(n)$, satisfying two conditions. The first condition is that $\alpha_x(n)$ has an even probability density function, i.e., positive and negative flip angles are equally likely. This implies that $\alpha_x(n)$ has a zero mean. For the case of non-zero mean excitation see reference (*21*). The second condition is that $\alpha_x(n)$ represents the random flip angles of the RF pulses with a mean square value of α^2 and

$$\langle \alpha_x(n)\,\alpha_x(m)\rangle = \alpha^2\,\delta_{nm}.$$

The matrix $\boldsymbol{R}_\alpha(n)$ is

$$
\boldsymbol{R}_\alpha(n) = \begin{bmatrix} 1 & 0 & 0 \\ 0 & \cos\alpha_x(n) & \sin\alpha_x(n) \\ 0 & -\sin\alpha_x(n) & \cos\alpha_x(n) \end{bmatrix},
$$

which represents a rotation of the magnetization vector about the x-axis of the rotating frame for $\alpha_x(n)$ degrees. The probability density function of $\alpha_x(n)$ is assumed to be even, so $\langle \sin \alpha_x(n) \rangle = 0$ and $\langle \cos \alpha_x(n) \rangle = \varphi_\alpha(1)$, where $\varphi_\alpha(t) = \langle e^{i\alpha_x(n)t} \rangle$ is the characteristic function of the random variable $\alpha_x(n)$. The characteristic function of a Gaussian white noise sequence satisfying the above conditions is $\varphi_\alpha(t) = e^{-\alpha^2 t^2/2}$. A random binary sequence taking on two values, α and $-\alpha$, each with probability 1/2 will also satisfy the above conditions. Its characteristic function is $\varphi_\alpha(t) = \cos(\alpha t)$.

The mean of the rotation matrix $\boldsymbol{R}_\alpha(n)$ is

$$\boldsymbol{\mu}_R = \begin{bmatrix} 1 & 0 & 0 \\ 0 & \varphi_\alpha(1) & 0 \\ 0 & 0 & \varphi_\alpha(1) \end{bmatrix}. \qquad [24]$$

Equation [7] gives the mean magnetization vector

$$\boldsymbol{\mu}_M = \frac{M_e(1-E_1)\,\varphi_\alpha(1)}{1-E_1\,\varphi_\alpha(1)} \begin{bmatrix} 0 \\ 0 \\ 1 \end{bmatrix}. \qquad [25]$$

The matrix $\boldsymbol{A}$ from Eq. [12] is

$$\boldsymbol{A} = \frac{-M_e(1-E_1)\,\dot{\varphi}_\alpha(1)}{1-E_1\,\varphi_\alpha(1)} \begin{bmatrix} 0 & 0 & 0 \\ 1 & 0 & 0 \\ 0 & 0 & 0 \end{bmatrix}, \qquad [26]$$

where $\dot{\varphi}_\alpha(1)$ is the first derivative of $\varphi_\alpha(t)$ evaluated at $t = 1$. Equation [15] can now be evaluated to give an estimate of the spectrum

$$K_1(\omega) = \frac{-i\,M_e(1-E_1)\dot{\varphi}_\alpha(1)}{\alpha^2[1-E_1\,\varphi_\alpha(1)]} \, \frac{1-E_2\,e^{i(\theta+\omega T_R)}}{D(\omega)} \qquad [27]$$

where

$$D(\omega) = 1 - E_2 \cos\theta\,[1+\varphi_\alpha(1)]\,e^{i\omega T_R} + E_2^2\,\varphi_\alpha(1)\,e^{2i\omega T_R}.$$

The first part of the right side of Eq. [27] is dependent on T_1 and the excitation power, but independent of ω and T_2. Define the second part as

$$F(\omega) = \frac{1 - E_2\, e^{i(\theta+\omega T_R)}}{D(\omega)}. \qquad [28]$$

$F(\omega)$ has T_2 dependence, but no T_1 dependence. The function $F(\omega)$ is periodic with a period of $2\pi/T_R$ rad/sec, or $1/T_R$ Hz. Integrating $F(\omega)$ over one period gives $2\pi/T_R$, which is independent of T_2 and the excitation power. Therefore, the integrated line intensity is purely determined by T_1, T_R and the excitation power. The line shape is determined only by T_2, T_R, θ and the excitation power. In conventional FT-NMR with T_R comparable to T_1, the integrated spectral intensity is also determined by T_1, T_R and the excitation power. However, the line shape is independent of θ, i.e., independent of resonance offset. Figure 4a shows the line shape (the absorption part) of $K_1(\omega)$ for Gaussian white noise excitations with different RMS flip angles, i.e. with different excitation power. Figure 4b is a plot of the corresponding integrated spectral intensity as a function of the RMS flip angle. The plot is normalized by the integrated spectral intensity at $\alpha = 0°$. This is made possible by the fact that $K_1(\omega)$ is well defined even when $\alpha = 0$. Figure 5 shows the shape of lines at different resonance offset frequencies. These plots show the following saturation characteristics: (1) At low excitation power the line shape resembles a Lorentzian line, (2) the line width (measured at half height) increases as the excitation power is increased, (3) spectral distortion appears at the negative of the resonance offset frequency as the excitation power is increased, (4) the integrated line intensity decreases rapidly as the excitation power is increased and (5) the response across the spectrum is non-uniform in the sense that a line at resonance has a width at half height different than a line off resonance.

To understand the saturation characteristics, consider the line shape function $F(\omega)$ defined in Eq. [28]. For both the Gaussian white noise sequence and the random binary sequence, $\varphi_\alpha(1)$

approaches unity as the excitation power α^2 approaches zero. $F(\omega)$ then reduces to

$$F_1(\omega) = \frac{1}{1 - E_2\, e^{i(\omega T_R - \theta)}} \qquad [29]$$

which approximate a Lorentzian line with line width $1/\pi T_2$ Hz. A Lorentzian line with the same line width is

$$\frac{1}{1 - i(\omega - \theta/T_R)T_2}.$$

Figure 6 shows that the only difference between $F_1(\omega)$ and the Lorentzian line is a slightly larger baseline offset in $F_1(\omega)$. The larger baseline offset is a consequence of aliasing due to under sampling of the random magnetization response. The narrower $F_1(\omega)$ is relative to the total bandwidth $1/T_R$, the smaller the baseline offset will be. This is usually the case in spectroscopy. Therefore, any line in the form of $F_1(\omega)$ will be referred to as a Lorentzian line in this paper. With the assumption that the interpulse dephase is only caused by the resonance offset, $\theta = 2\pi\nu T_R$, the line is centered at ν Hz. The reconstructed spectrum at low excitation power, e.g. the line with $\alpha = 1.15°$ in Fig. 4, resembles that obtained by a conventional FT-NMR.

As the excitation power is increased, $\varphi_\alpha(1)$ decreases from unity. The line shape becomes dependent on the resonance offset, ν. Figure 5 shows the shape of the absorption part of $K_1(\omega)$ for lines at different resonance offsets. When the line is on resonance, i.e. $\theta = 0$, $F(\omega)$ reduces to

$$F_2(\omega) = \frac{1}{1 - E_2\, \varphi_\alpha(1)\, e^{i\omega T_R}} \qquad [30]$$

which is also a Lorentzian line centered at the origin. The line width in Hertz is now increased to

$$\frac{1}{\pi T_2} - \frac{1}{\pi T_R} \log \varphi_\alpha(1). \qquad [31]$$

For lines not at resonance, $F(\omega)$ cannot be simplified. At $\omega = -\theta/T_R$, the numerator of $F(\omega)$ reduces to $(1 - E_2)$. In general T_R is much smaller than T_2, as a result E_2 is very close to unity and $F(\omega)$ vanishes at $\omega = -\theta/T_R$, the negative of the resonance offset. This creates a notch artifact for

lines with a resonance offset which is small relative to the line width (Fig. 5). When the resonance offset is large relative to the line width and such that

$$\cos\theta < \frac{2\sqrt{\varphi_\alpha(1)}}{1+\varphi_\alpha(1)}, \qquad [32]$$

the notch artifact becomes less significant. However, the line shape is now given by

$$F_3(\omega) \propto \frac{1}{1 - E_2\sqrt{\varphi_\alpha(1)}\, e^{i(\omega T_R - \theta')}} \qquad [33]$$

where

$$\theta' = \cos^{-1}\left[\cos\theta \frac{1+\varphi_\alpha(1)}{2\sqrt{\varphi_\alpha(1)}}\right].$$

The line is Lorentzian centered at a new resonance offset $\nu' = \theta'/2\pi T_R$. The line width in Hertz is

$$\frac{1}{\pi T_2} - \frac{1}{2\pi T_R}\log\varphi_\alpha(1), \qquad [34]$$

which means that the line broadening is half that of the line at resonance. Consequently, the line height is about twice that at resonance (Fig. 5). For Gaussian white noise excitation and random binary excitation, the function $\varphi_\alpha(1)$ is smaller than unity for $\alpha < 90°$ and is a monotonically decreasing function of α. Equations [31] and [34] show that the line width at half height increases as the excitation power, α, is increased.

The foregoing results explain the discrepancy between the results obtained by Bartholdi *et al.* (*17*) and those of Knight & Kaiser (*9*). Bartholdi *et al.* analyzed the experiment with continuous Gaussian white noise excitation. However, they did so only for spins at resonance. They obtained a Lorentzian line with a line broadening of $\sigma^2/2\pi$ Hz, where σ^2 is the excitation power per unit time. In the analysis above, a Gaussian white noise excitation has $\varphi_\alpha(1) = e^{-\alpha^2/2}$. Assume T_R to be very small relative to T_1 and define $\sigma^2 = \alpha^2/T_R$, Eq. [31] then gives the same line broadening for spins at resonance. Knight and Kaiser also obtained results based on continuous excitation. However, they used a laboratory frame where each spin is offset by its Larmor precession frequency. They

obtained a small line shift and a line broadening of $\sigma^2/4\pi$ Hz. For spins off resonance, Eq. [34] gives the same line broadening and Eq. [33] also predicts the same line shift. The results of the two groups of researchers are different halves of the complete solution.

For the analysis of the average signal power write $\langle M\, M^T\rangle$ as

$$\langle M\, M^T\rangle = \begin{bmatrix} r_{xx} & r_{xy} & r_{xz} \\ r_{xy} & r_{yy} & r_{yz} \\ r_{xz} & r_{yz} & r_{zz} \end{bmatrix}.$$

The individual components are obtained by solving Eq. [17]:

$$r_{xx} = M_e^2(1-E_1)^2\,\frac{1+E_1\,\varphi_\alpha(1)}{1-E_1\,\varphi_\alpha(1)}\,\frac{E_2^2\sin^2\theta(1-\varphi_\alpha(2))(1+E_2^2\,\varphi_\alpha(1))}{2Q}, \qquad [35]$$

$$r_{xy} = M_e^2(1-E_1)^2\,\frac{1+E_1\,\varphi_\alpha(1)}{1-E_1\,\varphi_\alpha(1)}\,\frac{E_2^2(1-E_2^2)\sin\theta\cos\theta\,\varphi_\alpha(1)(1-\varphi_\alpha(2))}{2Q}, \qquad [36]$$

$$r_{yy} = M_e^2(1-E_1)^2\,\frac{1+E_1\,\varphi_\alpha(1)}{1-E_1\,\varphi_\alpha(1)} \times\frac{(1-\varphi_\alpha(2))(1-E_2^2\cos^2\theta-E_2^2\cos 2\theta\,\varphi_\alpha(1)+E_2^4\cos^2\theta\,\varphi_\alpha(1))}{2Q} \qquad [37]$$

and

$$r_{xz} = r_{yz} = 0 \qquad [38]$$

where

$$\begin{aligned} Q = {} & (1-E_2^2)(1-E_2^2\cos 2\theta\,\varphi_\alpha(1))[1-\frac{1}{2}(E_1^2+E_2^2)(1+\varphi_\alpha(2))+E_1^2E_2^2\,\varphi_\alpha(2)] \\ & +2E_2^2(1-E_2^2)\sin^2\theta(1+E_2^2\,\varphi_\alpha(1))[\frac{1}{2}(1+\varphi_\alpha(2))-E_1^2\,\varphi_\alpha(2)] \\ & +\frac{1}{2}E_2^2(1-E_1^2)\sin^2\theta(1-\varphi_\alpha(2))(1+E_2^2\,\varphi_\alpha(1)). \end{aligned} \qquad [39]$$

The expression for r_{zz} is not shown since it is not required for the ensuing analysis. The average signal power is given by $P = r_{xx} + r_{yy}$.

Figure 7a is a plot of the average signal power as a function of the RMS flip angle α of a Gaussian white noise excitation. It has a peak at 1.15°. This means that the S/N ratio is at a

maximum when the excitation sequence has a RMS flip angle of 1.15°. Notice that the S/N ratio is independent of the spectral resolution. Define α_{max} as the RMS flip angle that gives the maximum S/N ratio. For the example in Fig. 7a α_{max} is only 1.15°. The integrated spectral intensity plot in Fig. 4b does not show a maximum response at α_{max}, because the spectral estimate $K_1(\omega)$ is defined to be normalized by the RF excitation power (Eq. [15]), while no such normalization is applied to the average signal power.

The Ernst angle is the flip angle that gives the maximum signal in a conventional FT-NMR experiment that consists of one RF excitation every T_R seconds. Figure 7b shows that α_{max} is approximately the Ernst angle, $\cos^{-1}(e^{-T_R/T_1})$. For the same spin system a conventional FT-NMR experiment with $T_R = 0.1$s will have an Ernst angle of 35°. The peak RF power is proportional to the square of the RF field strength, i.e., the square of the flip angle. Therefore, the peak power required for the stochastic experiment is roughly three orders of magnitude smaller than that for the conventional FT-NMR experiment.

In many cases T_R is much shorter than T_1, so α_{max} will be less than 10° and $\varphi_\alpha(1)$ very close to unity. The notch artifact is usually insignificant at this low level of excitation. However, for T_2 large such that the natural line width, $1/\pi T_2$, is small compared with the line broadening, $\log \varphi_\alpha(1)/\pi T_R$, at $\alpha = \alpha_{max}$, the difference in line broadening between on resonance and off resonance lines may still be large. To minimize this non-uniform response, the excitation level must be dropped below α_{max}, resulting in a lower S/N ratio.

It is important to recognize that a hard pulse assumption has not been required in the treatment presented here. The only requirement of the RF pulse is that of short duration so that the RF bandwidth is large compared to the chemical shift range of interest. When this requirement is not satisfied, there will be errors in the RF flip angle. For example, when the chemical shift range

of interest is 15% of the RF bandwidth, the maximum error in the flip angle is 1% and the phase error in the transverse magnetization after the RF pulse is linear across the spectrum from $-15°$ to $15°$. These errors are independent of the RF flip angle. Theoretical derivation of $K_1(\omega)$ with the flip angle errors incorporated into the RF rotation matrix $\boldsymbol{R}_\alpha(n)$ is straightforward and will not be shown here. The results show that the only effect of these errors is to introduce a linear phase into $K_1(\omega)$, which can be corrected easily.

To evaluate the signal power spectrum as an estimate of the spectrum Eqs. [22] and [23] are made specific for random flip angle excitation to give

$$\begin{aligned} S(\omega) &= \frac{P - E_2 e^{i(\theta+\omega T_R)}[r_{xx}\,\varphi_\alpha(1) + r_{yy} + i r_{xy}(1-\varphi_\alpha(1))]}{D(\omega)} \\ &\quad + \frac{P - E_2 e^{-i(\theta+\omega T_R)}[r_{xx}\,\varphi_\alpha(1) + r_{yy} - i r_{xy}(1-\varphi_\alpha(1))]}{D(\omega)^*} - P. \end{aligned} \qquad [40]$$

The power spectrum shown in Fig. 8a closely resembles the absorption part of $K_1(\omega)$ (Fig. 4a) at low excitation power. At higher excitation power, the notch artifact is less prevalent. An advantage of using the spectral density as an estimate of the real spectrum is that it is calculated from the signal sequence only, so that the excitation sequence $\alpha(n)$ need not be stored or regenerated. However, as shown in Fig. 8b, the response is still non-uniform across the spectrum. It will be shown in Part II (*18*) that the non-uniform response can be eliminated with a different excitation scheme.

Another undesirable property associated with signal power spectra is non-additivity. The derivation for $S(\omega)$ in Eqs. [18]-[23] is rigorous only for an isolated line. When there are two or more lines in the spectrum, cross products of the transverse magnetization must be included in Eq. [18]. The derivation of the cross product terms is very similar to that for $r(m)$, however, the results are much more complicated and will not be shown here. The results show that the cross product terms are significant only in regions where there is significant overlap of lines. When two lines are far apart, the contributions of the cross product terms are centered at the resonance offset frequencies of the two participating lines and are less than 1%.

So far only results for Gaussian white noise excitations have been considered. The dependence of $K_1(\omega)$, P and $S(\omega)$ on the type of excitation that is used is embedded in $\varphi_\alpha(1)$, $\varphi_\alpha(2)$ and $\dot{\varphi}_\alpha(1)$. Power series expansion shows that the differences in these functions between Gaussian white noise excitation and random binary excitation are

$$\Delta\varphi_\alpha(1) = \frac{\alpha^4}{12}\left(1 - \frac{7\alpha^2}{30} + \cdots\right),$$

$$\Delta\varphi_\alpha(2) = \frac{4\alpha^4}{3}\left(1 - \frac{14\alpha^2}{15} + \cdots\right) \text{ and}$$

$$\Delta\dot{\varphi}_\alpha(1) = \frac{\alpha^4}{3}\left(1 - \frac{7\alpha^2}{20} + \cdots\right)$$

where $\Delta\varphi_\alpha(t)$ = Gaussian $\varphi_\alpha(t)$ − Binary $\varphi_\alpha(t)$. For $\alpha = \alpha_{max} < 0.175$ rad $(= 10°)$ the fractional differences, $\Delta\varphi_\alpha(1)/\varphi_\alpha(1)$, $\Delta\varphi_\alpha(2)/\varphi_\alpha(2)$ and $\Delta\dot{\varphi}_\alpha(1)/\dot{\varphi}_\alpha(1)$, are negligible. This means that the response to Gaussian white noise excitation and random binary excitation will be almost identical.

Experimental Verification

To verify the theoretical results in the previous sections, stochastic NMR experiments were performed on a 0.5T whole body imaging system. The analysis that has been presented is independent of field strength, and the results will be applicable to studies at any field strengths. As discussed earlier, except at large flip angles, random binary excitation and Gaussian white noise excitation give almost identical responses. The hardware implementation of a Gaussian white noise sequence is substantially more difficult than MLS. Therefore results obtained with binary MLS excitation will be presented. The 0.5T whole body imaging system was developed by IBM Corporation, Massachusetts Institute of Technology and Lawrence Berkeley Laboratory. The spectrometer design allows many different types of NMR experiments, including stochastic NMR, to be performed

with very few hardware modifications. All experiments were performed at the proton frequency of 21MHz.

The RF transmitter has 16 2-word ECL registers that determine the magnitude and phase of an RF pulse. These registers are loaded by software and selected using four TTL digital logic lines. These four lines are usually driven by the pulse programmer which compiles and runs the pulse program. To implement stochastic NMR with binary MLS excitation, a circuit was built to interpose two 31-bit MLS generators between the pulse programmer and transmitter. The 31-bit MLS generator was a 31-bit shift register with the exclusive-OR of the 3^{rd} bit and the 31^{st} bit fed back to form the first bit (*19*). One pseudo-random binary number was generated at the output of the 31^{st} shift register after every clock pulse.

The sample was a 10cm sphere filled with copper sulphate doped water. The T_1 and T_2 of the sample were measured to be 160ms and 140ms respectively (using conventional NMR techniques). However, due to the static field inhomogeneity (1ppm), the effective T_2, T_2^*, is 45ms. All experiments used a T_R of 200μs, which gave an optimum RMS flip angle of about 2.8°. The duration of the RF pulse was 25μs, corresponding to an excitation bandwidth of about 40kHz. The width of the reconstructed spectrum was $1/T_R$ = 5kHz, i.e., 12.5% of the RF bandwidth. Spins at large resonance offset would experience RF flip errors. The reconstructed $K_1(\omega)$ was therefore phase corrected to remove the linear phase resulted from the RF flip errors. The flip angles of the RF pulses were calibrated by a conventional NMR experiment. The excitation sequence has a length of N(=65536) which is a very small fraction of the period of the 31-bit MLS ($2^{31} - 1$). Such a sub-sequence behaves like a random binary sequence.

Initial results showed that there was an unexpected component with a very broad line width in addition to the resonance due to the aqueous solution. The broad component was significant

only when the excitation power was high, i.e., when the line from the copper sulphate solution was highly saturated and gave very little signal. This component was attributed to plastic in the probe assembly and was subtracted from all subsequent studies to correct the baseline

Figure 9 is a plot of the average signal power as a function of the RMS flip angle. The symbol * represents experimental data and the solid line is the corresponding theoretical prediction. The plot shows good agreement between theory and experiment. The analysis in earlier sections showed that there will be line broadening and a notch artifact in $K_1(\omega)$ as the excitation power is increased. Figure 10 is a side-by-side comparison of experimental and theoretical line shapes of $K_1(\omega)$. There are three important features of the spectra that should be noticed: (1) the line width, (2) the notch artifact and (3) the noise-like distortions. The experimental line broadens and the notch artifact gets worse as the RMS flip angle is increased, as predicted in Fig. 10b for random binary flip angle excitation. The noise-like distortion increases as the RMS flip angle increases in agreement with Blümich and Ziessow's observations (*10*). The analysis in Part II (*18*) will show that the noise-like distortion is due to undesirable third and higher order auto-correlations of the MLS and can be reduced by using a different MLS generator.

Theoretical analysis showed that the signal power spectrum has less notch artifact than $K_1(\omega)$. Figure 11a shows the signal power spectra of the same data sets used to obtain $K_1(\omega)$ in Fig. 10a. They show good agreement with the theoretical predictions shown in Fig. 10b except for a DC offset that will be shown in Part II (*18*) to result from the measurement noise. The notch artifact is indeed smaller than that in $K_1(\omega)$. It is very interesting to notice that the signal power spectrum shows significantly less noise-like distortion even when the excitation power is very high. This may be another advantage of the signal power spectrum over $K_1(\omega)$ as an estimate of the real spectrum.

Conclusions

The discrete stochastic NMR experiment in Fig. 2 has been analyzed. Closed form expressions for the first order input-output cross-correlation, the average signal power and the signal power spectrum have been obtained for a generalized RF excitation sequence. These expressions were made specific for random flip angle excitations. They show that, at very low excitation power level, the spin system behaves linearly and the first order input-output cross-correlation is a faithful estimate of the FID obtained from a conventional FT-NMR experiment. However, when the excitation power is high, the reconstructed spectral estimate $K_1(\omega)$ has a notch artifact at the negative of the resonance offset and the response across the spectrum is non-uniform, i.e., the line broadening depends on the resonance offset. The amount of spectral distortion increases with excitation power.

The plot of the average signal power as a function of the RMS flip angle for the random flip angle excitation, Fig. 9, shows that the RMS flip angle that maximizes the S/N ratio, α_{max}, is usually much smaller than that for conventional FT-NMR. This allows a reduction by several orders of magnitude in the peak RF power required for the stochastic NMR experiment. The optimal flip angle α_{max} is approximately given by the Ernst angle formula. The major drawback of the random flip angle excitation is that α_{max} can be large enough to invoke a nonlinear response which results in a non-uniform response across the spectrum. Consequently the S/N ratio must be sacrificed in order to avoid spectral distortion.

The power spectrum resembles the absorption part of $K_1(\omega)$ but with much less notch artifact. The power spectrum can be calculated directly from the signal sequence, and so the excitation sequence need not be stored or regenerated. Experimental results show that it is much less sensitive to the undesirable characteristics of the higher auto-correlations of the maximum length sequences (MLS) and hence shows much less noise-like distortion than $K_1(\omega)$. However, it still exhibits a non-uniform spectral response and it is non-additive.

Theoretical analysis shows that, at low excitation power levels, the performance of random binary sequences and Gaussian white noise sequences is almost identical. This is desirable since the random binary sequence can be approximated by MLS which are easy to generate both with hardware and software.

Random flip angle excitation produces spectral distortions that force a sacrifice of the S/N ratio of the reconstructed spectrum. Part II (*18*) will show that most of these distortions can be removed by randomizing the phase of the RF vector.

Acknowledgements

This work was supported in part by the Whittaker Foundation (M.S. Roos) and the U.S. Department of Energy under contract No. DE-AC03-76SF00098.

References

1. R. R. Ernst, *J. Chem. Phys.* **45**, 3845(1966).

2. R. R. Ernst, *J. Magn. Reson.* **3**, 10(1970).

3. D. Ziessow, "On-line Rechner in der Chemie, Grundlagen und Anwendung in der Fourier-spektroskopie", Walther de Gruyter, Berlin, 1973.

4. D. Ziessow and B. Blümich, *Ber. Bunsenges. Phys. Chem.* **78**, 1169(1974).

5. R. Kaiser, *J. Magn. Reson.* **3**, 28(1970).

6. B. Blümich and D. Ziessow, *Ber. Bunsenges. Phys. Chem.* **84**, 1090(1980).

7. R. Kaiser, *J. Magn. Reson.* **15**, 44(1974).

8. R. Kaiser and W. R. Knight, *J. Magn. Reson.* **50**, 467(1982).

9. W. R. Knight and R. Kaiser, *J. Magn. Reson.* **48**, 293(1982).

10. B. Blümich and D. Ziessow, *J. Magn. Reson.* **46**, 385(1982).

11. B. Blümich and D. Ziessow, *J. Magn. Reson.* **52**, 42(1983).

12. B. Blümich and R. Kaiser, *J. Magn. Reson.* **54**, 486(1983).

13. B. Blümich and D. Ziessow, *Molec. Phys.* **48**, 955(1983).

14. B. Blümich and D. Ziessow, *Molec. Phys.* **48**, 969(1983).

15. B. Blümich and D. Ziessow, *J. Chem. Phys.* **78**, 1059(1983).

16. B. Blümich, *Molec. Phys.* **51**, 1283(1984).

17. E. Bartholdi, A. Wokaun and R. R. Ernst, *Chem. Phys.* **18**, 57(1976).

18. S. T. S. Wong, M. S. Roos, R. D. Newmark and T. F. Budinger, in preparation.

19. W. H. Press, B. P. Flannery, S. A. Teukolsky and W. T. Vetterling, "Numerical Recipes, The Arts of Scientific Computing", Cambridge University Press, 1986.

20. D. E. Knuth, "The Art of Computer Programming", Volume 2, Addison-Wesley, 1981.

21. S. T. S. Wong, "Discrete Analysis of Stochastic NMR", Ph.D. thesis, University of California, San Francisco, December 1988.

Figure Captions

Figure 1 (a) Identification of the impulse response $h(t)$ of a linear system by the cross-correlation of the input $x(t)$ and the output $y(t)$ of the system. (b) The same principle applied to the stochastic spectroscopy experiment and spectral estimation.

Figure 2 Scheme for RF excitation and Data acquisition during a NMR experiment with discrete stochastic RF excitation.

Figure 3 Block diagram of the approach taken for the theoretical analysis.

Figure 4 $K_1(\omega)$ for random flip angle excitation with Gaussian white noise. (a) Line shape (absorption part) and (b) integrated line intensity normalized by the value at $\alpha = 0°$. $T_1 = 0.5$s, $T_2 = 10$ms, $T_R = 0.1$ms and $\nu = 250$Hz.

Figure 5 Line shape of $K_1(\omega)$ with different resonance offset frequencies. The excitation is Gaussian white noise random flip angle excitation with $\alpha = 15°$. $T_1 = 0.5$s, $T_2 = 10$ms and $T_R = 0.1$ms. All the plots are on the same vertical scale.

Figure 6 A comparison of the line shape of $[1 - E_2 e^{i\omega T_R}]^{-1}$ (dotted line) with a Lorentzian line with the same line width (solid line).

Figure 7 Random flip angle excitation with Gaussian white noise. (a) Average signal power versus the RMS flip angle. (b) α_{max} versus T_1/T_R. The symbol * represents theoretical values and the solid line is $\cos^{-1}(e^{-T_R/T_1})$. $T_1 = 0.5$sec, $T_2 = 10$ms, $T_R = 0.1$ms and $\nu = 250$Hz.

Figure 8 Power spectrum $S(\omega)$ for Gaussian white noise random flip angle excitation. $T_1 = 0.5$s and $T_R = 0.1$ms. (a) $S(\omega)$ with different RMS flip angles. $\nu = 250$Hz and $T_2 = 10$ms. The plots have different vertical scale. (b) $S(\omega)$ for 11 evenly spaced resonances. $\alpha = 1.15°$ and $T_2 = 100$ms.

Figure 9 Average signal power for random binary flip angle excitation. The excitation sequence is a sub-sequence of a 31-bit MLS generator. The symbol * represents experimental data point and the solid line is the theoretical prediction. $T_1 = 160$ms, $T_2^* = 45$ms, $T_R = 0.2$ms and $\nu = 500$Hz.

Figure 10 Line shapes of $K_1(\omega)$ for random binary flip angle excitation. (a) Experimental results using a 31-bit MLS generator and (b) theoretical predictions with random binary sequences. $T_1 = 160$ms, $T_2^* = 45$ms, $T_R = 0.2$ms, $N = 65536$ and $\nu = 60$Hz.

Figure 11 Signal power spectrum for random binary flip angle excitation. (a) Experimental results using a 31-bit MLS generator and (b) theoretical predictions with random binary sequences. $T_1 = 160$ms, $T_2^* = 45$ms, $T_R = 0.2$ms, $N = 65536$ and $\nu = 60$Hz.

Symbols

o	oh
O	uppercase oh
0	zero
l	ell
1	one
k	lowercase kay
K	uppercase kay
n^{th}	italic n superscript italic th
T_1	italic tee subscript 1
T_2	italic tee subscript 2
θ	theta (Greek)
μ	mu (Greek)
μ_x	mu (Greek) subscript italic x
$\boldsymbol{\mu}_\alpha$	bold mu (Greek) subscript alpha (Greek), a vector
$\boldsymbol{\mu}_M$	bold mu (Greek) subscript italic M
$\boldsymbol{\mu}_R$	bold mu (Greek) subscript italic R
α	alpha (Greek)
α_x	alpha (Greek) subscript italic x
$\boldsymbol{\alpha}$	bold alpha (Greek), a vector
ω	omega (Greek)
δ_{nm}	delta (Greek) subscript italic nm
Δ	upper case delta (Greek)
φ_α	variation of phi (Greek) subscript alpha (Greek)
π	pi (Greek)

ν	nu (Greek)
σ	sigma (Greek)
$\boldsymbol{A}$	bold A
$\boldsymbol{B}$	bold B
$\boldsymbol{C}$	bold C
$\boldsymbol{C}_{\alpha}$	bold C subscript alpha (Greek)
$\boldsymbol{M}$	bold, italic M, a vector
M_{xy}	italic M subscript italic xy
$\boldsymbol{R}_{\alpha}$	bold R subscript alpha (Greek), a matrix
$\boldsymbol{R}_{\theta}$	bold R subscript theta (Greek)
$\mathcal{Z}$	calligraphic Z

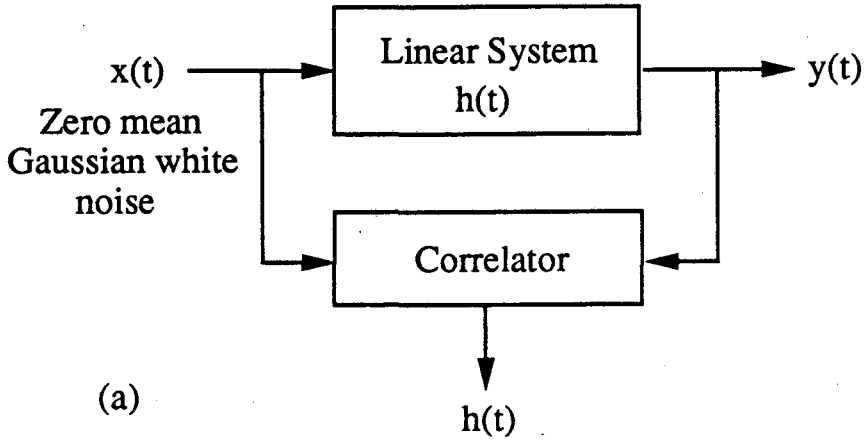
x(t)
Zero mean
Gaussian white
noise
Linear System
h(t)
y(t)
Correlator
h(t)

(a)

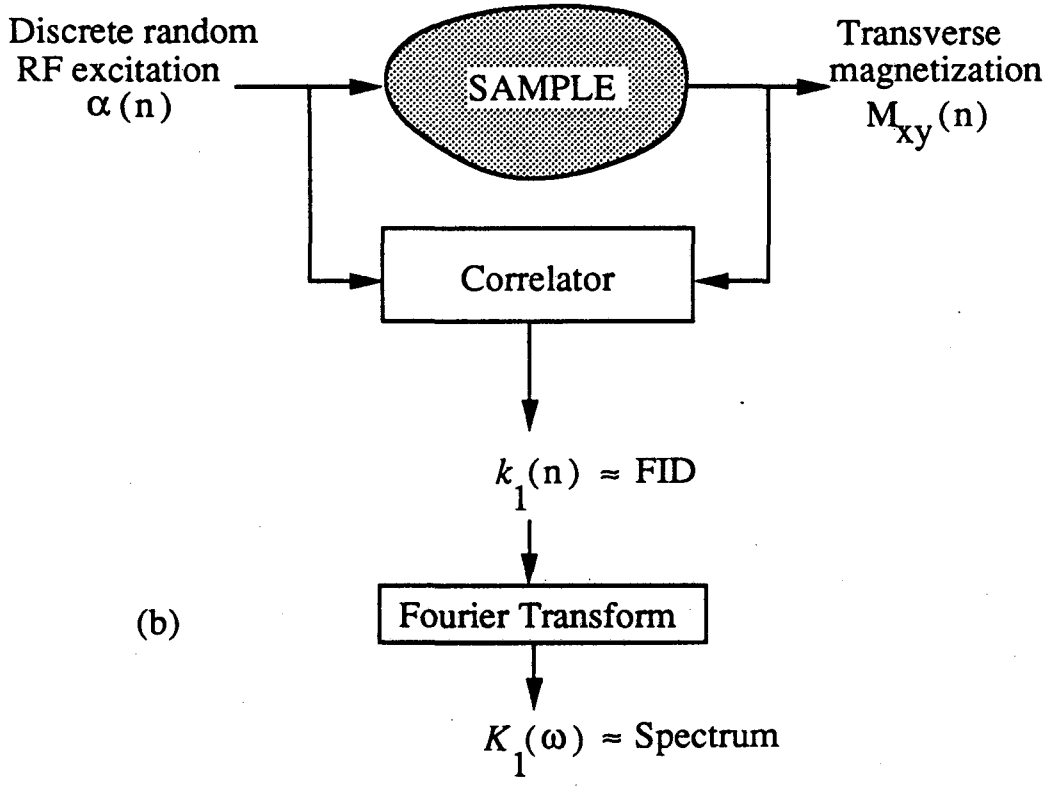
Discrete random
RF excitation
α(n)
SAMPLE
Transverse
magnetization
$M_{xy}(n)$
Correlator
$k_1(n) \approx$ FID
Fourier Transform
$K_1(\omega) \approx$ Spectrum

(b)

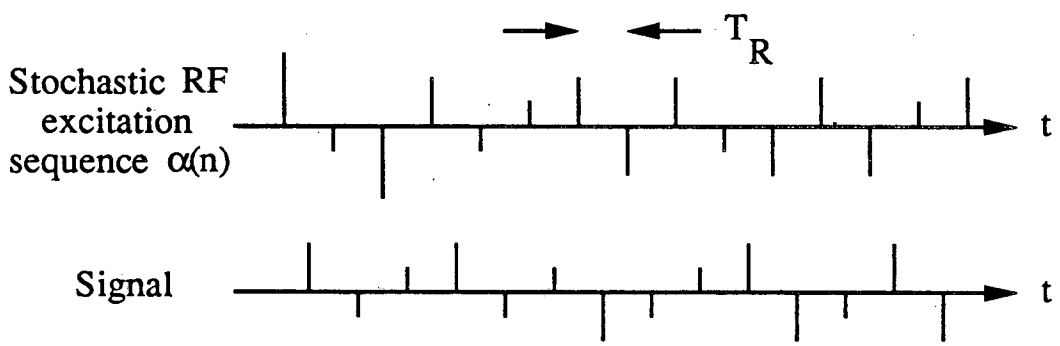
T_R
Stochastic RF
excitation
sequence α(n)
t
Signal
t

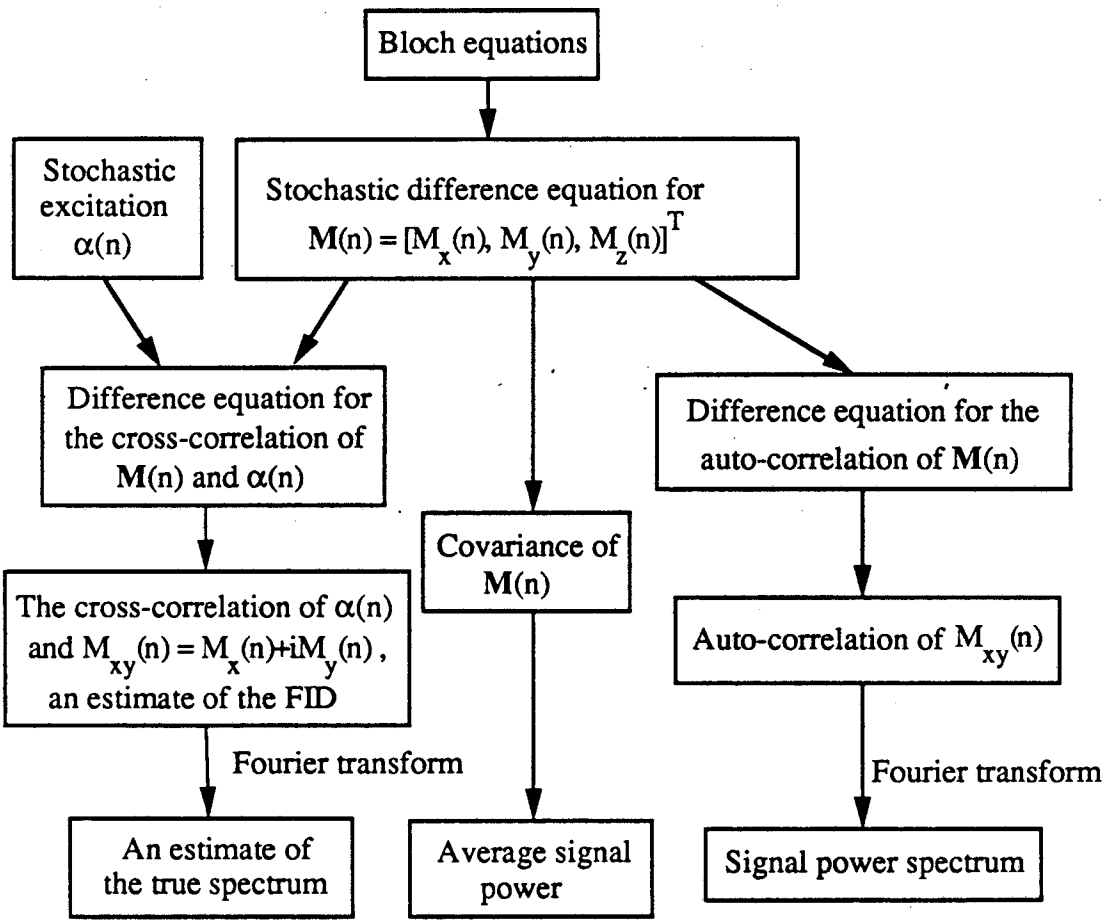
Bloch equations
Stochastic excitation α(n)
Stochastic difference equation for M(n) = [M_x(n), M_y(n), M_z(n)]^T
Difference equation for the cross-correlation of M(n) and α(n)
Covariance of M(n)
Difference equation for the auto-correlation of M(n)
The cross-correlation of α(n) and M_xy(n) = M_x(n)+iM_y(n), an estimate of the FID
Auto-correlation of M_xy(n)
Fourier transform
Fourier transform
An estimate of the true spectrum
Average signal power
Signal power spectrum

(a)

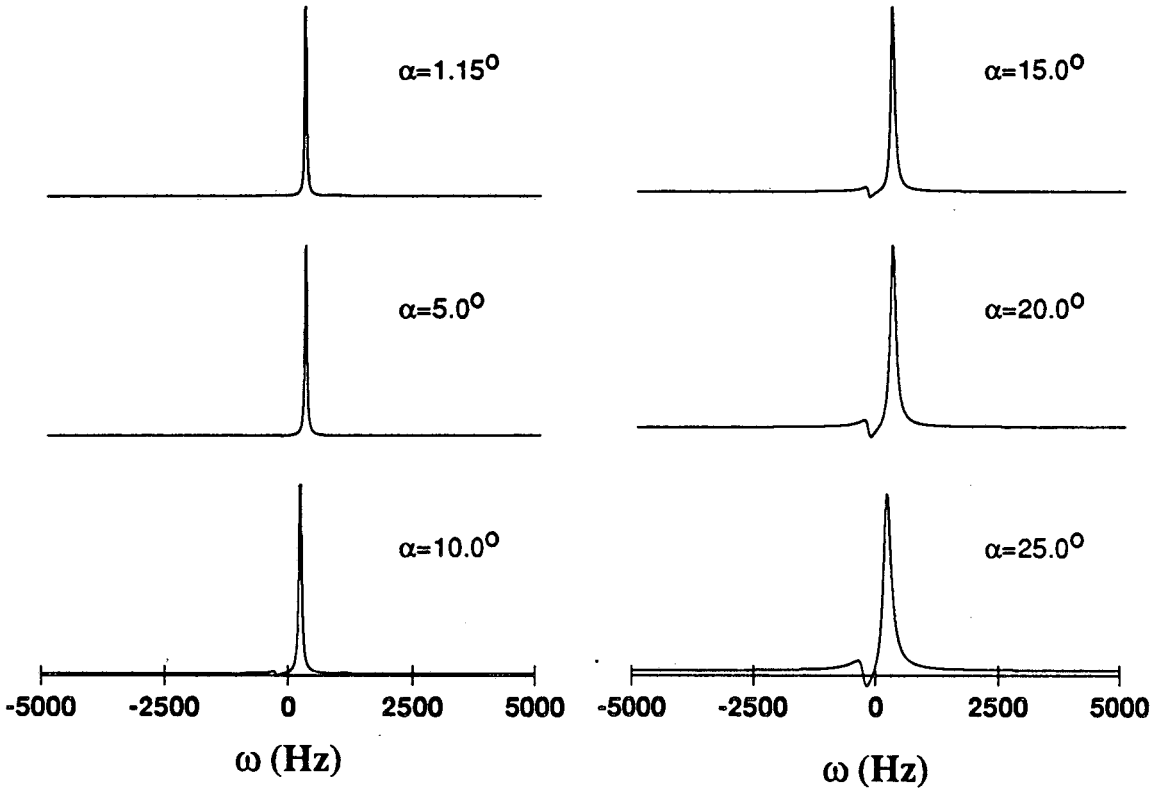
α=1.15°
α=15.0°
α=5.0°
α=20.0°
α=10.0°
α=25.0°
-5000
-2500
0
2500
5000
ω (Hz)
-5000
-2500
0
2500
5000
ω (Hz)

(b)

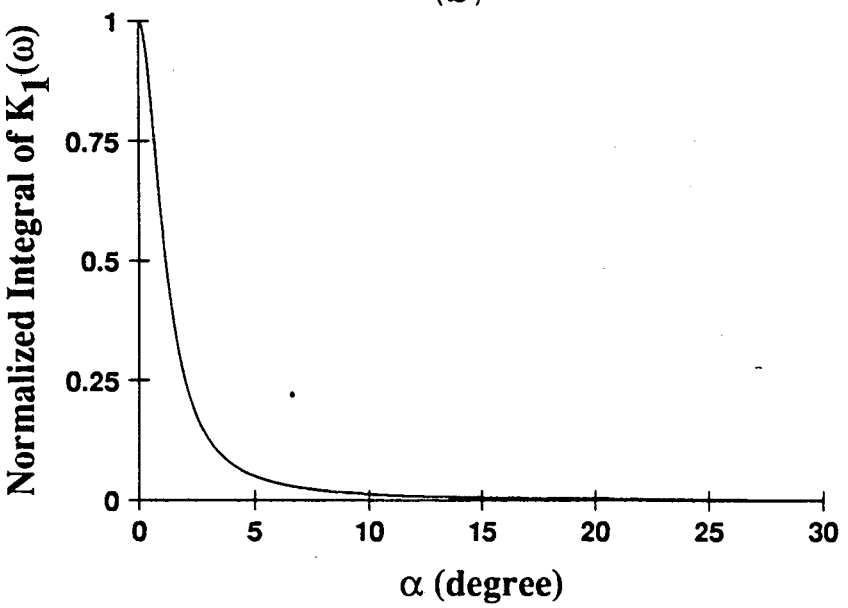
Normalized Integral of $K_1(\omega)$
1
0.75
0.5
0.25
0
0
5
10
15
20
25
30
α (degree)

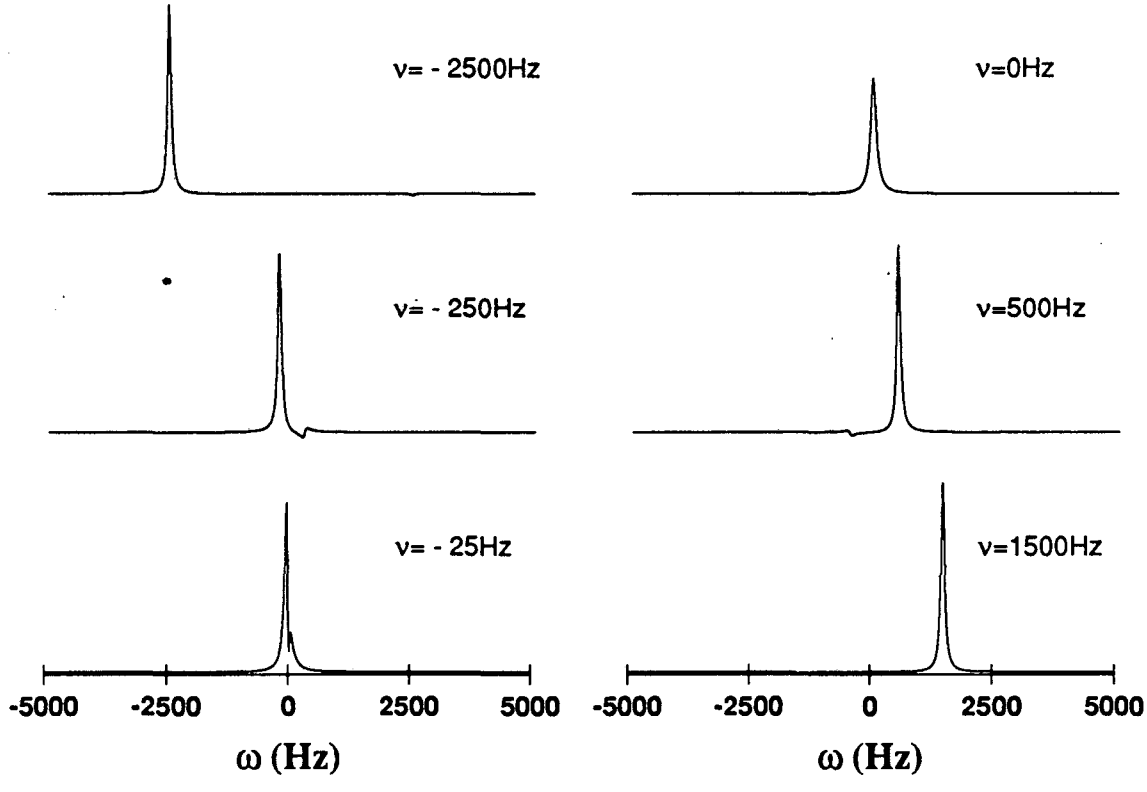
ν= - 2500Hz
ν=0Hz
ν= - 250Hz
ν=500Hz
ν= - 25Hz
ν=1500Hz
-5000
-2500
0
2500
5000
ω (Hz)
-5000
-2500
0
2500
5000
ω (Hz)

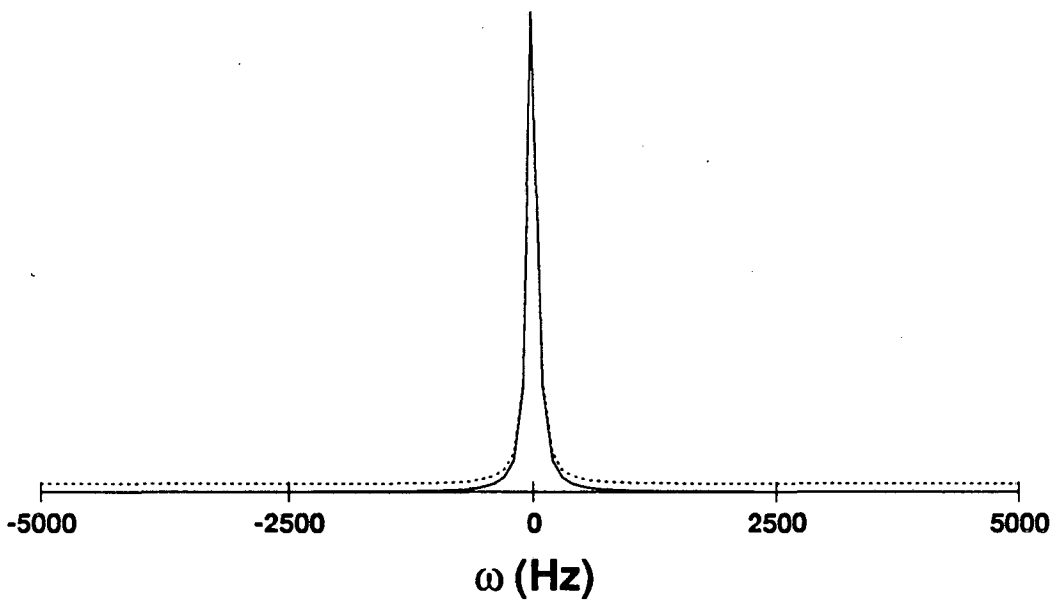
-5000
-2500
0
2500
5000
ω (Hz)

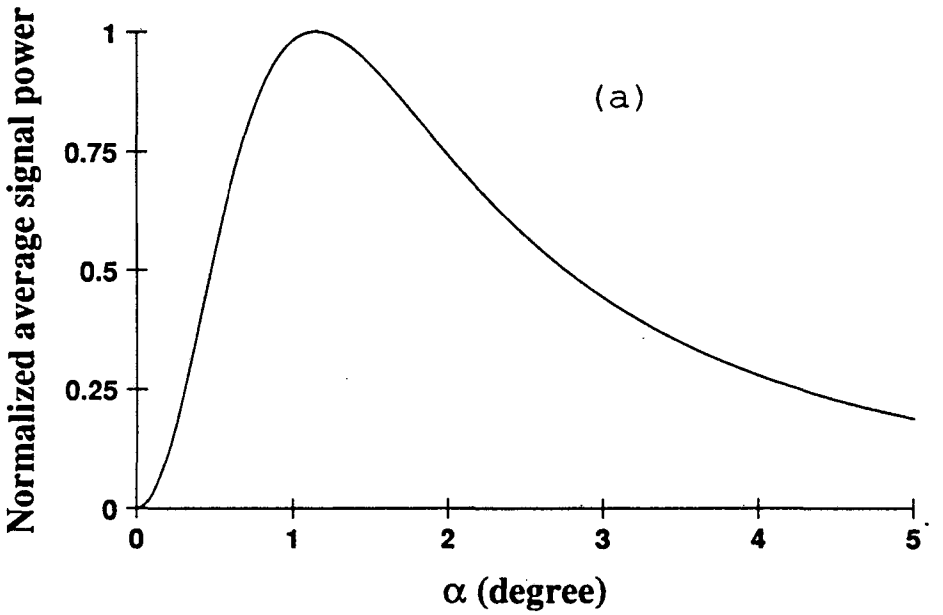
Normalized average signal power
1
0.75
0.5
0.25
0
0
1
2
3
4
5
α (degree)
(a)

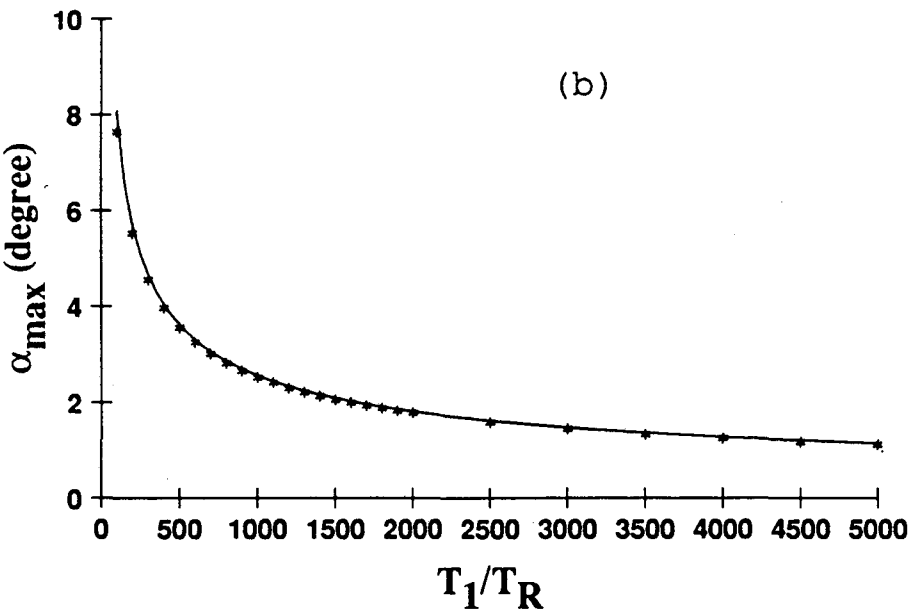
(b)
α_{max} (degree)
10
8
6
4
2
0
0
500
1000
1500
2000
2500
3000
3500
4000
4500
5000
T_1/T_R

(a)

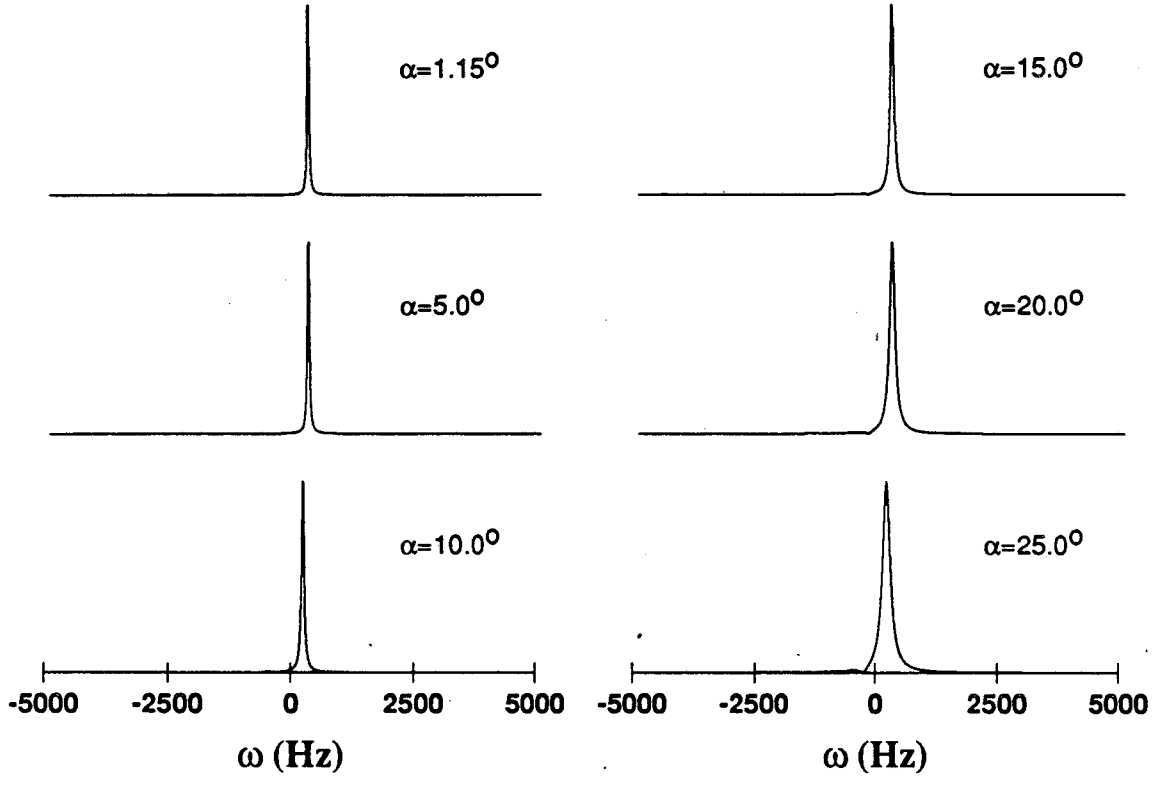
α=1.15°
α=15.0°
α=5.0°
α=20.0°
α=10.0°
α=25.0°
-5000
-2500
0
2500
5000
ω (Hz)

(b)

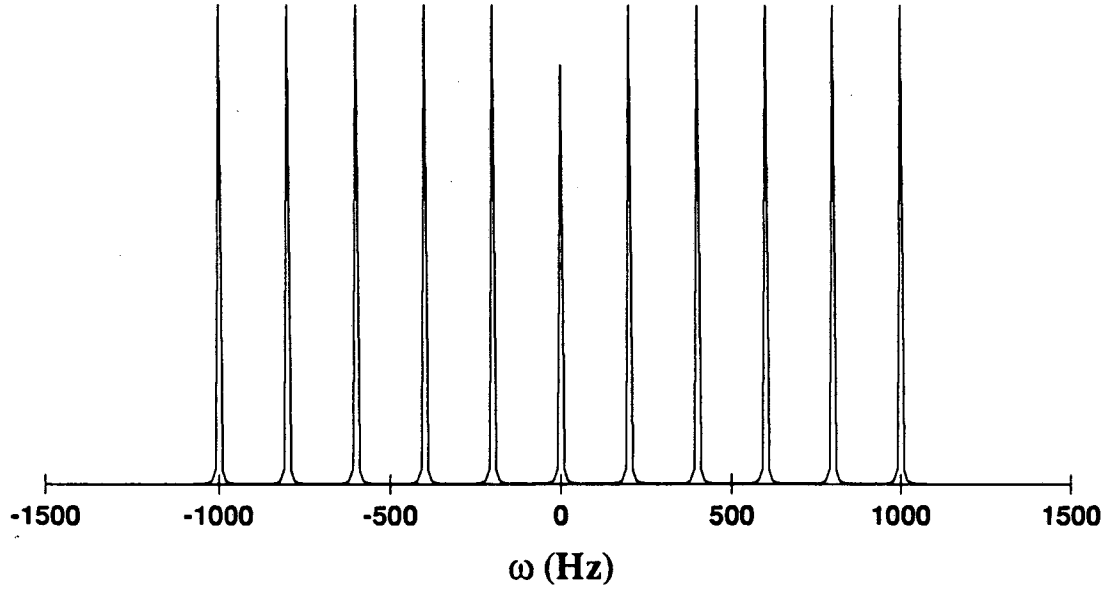
-1500
-1000
-500
0
500
1000
1500
ω (Hz)

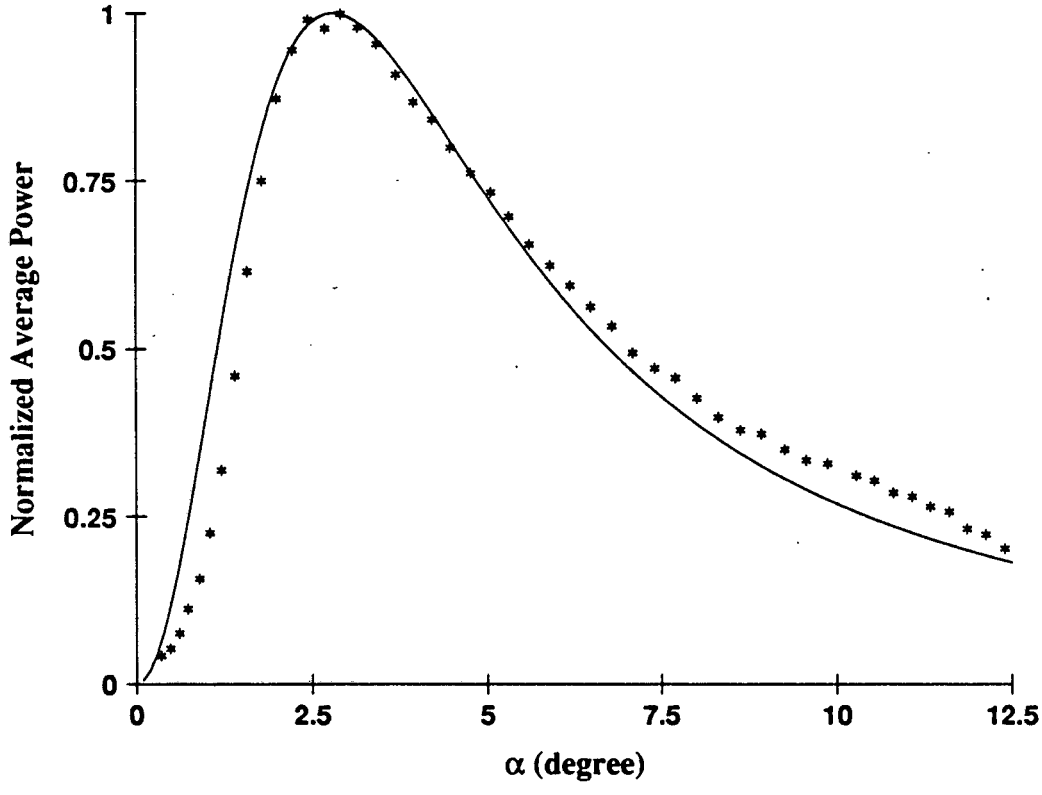
Normalized Average Power
1
0.75
0.5
0.25
0
0
2.5
5
7.5
10
12.5
α (degree)

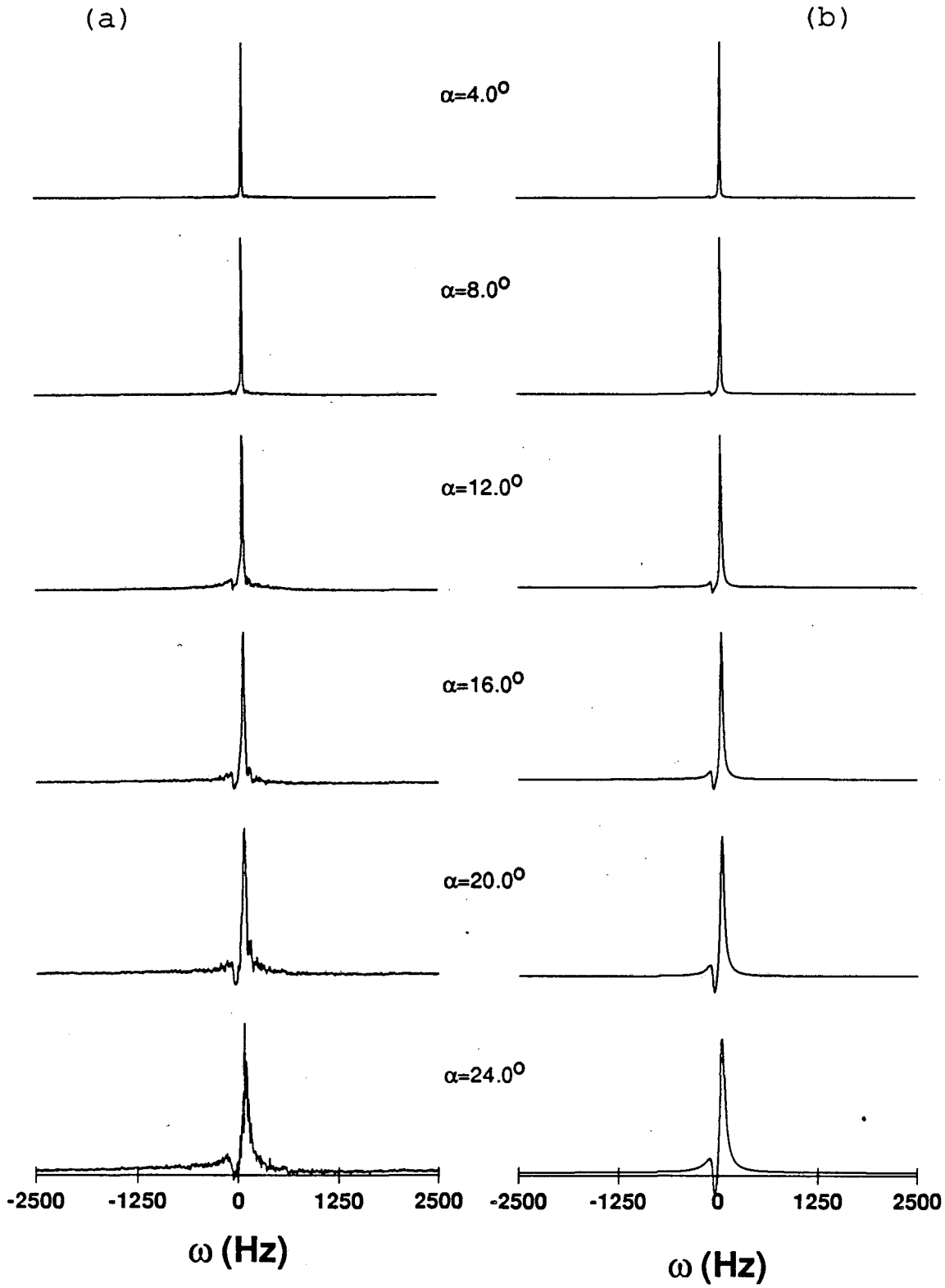
(a)
(b)
α=4.0°
α=8.0°
α=12.0°
α=16.0°
α=20.0°
α=24.0°
-2500
-1250
0
1250
2500
ω (Hz)
-2500
-1250
0
1250
2500
ω (Hz)

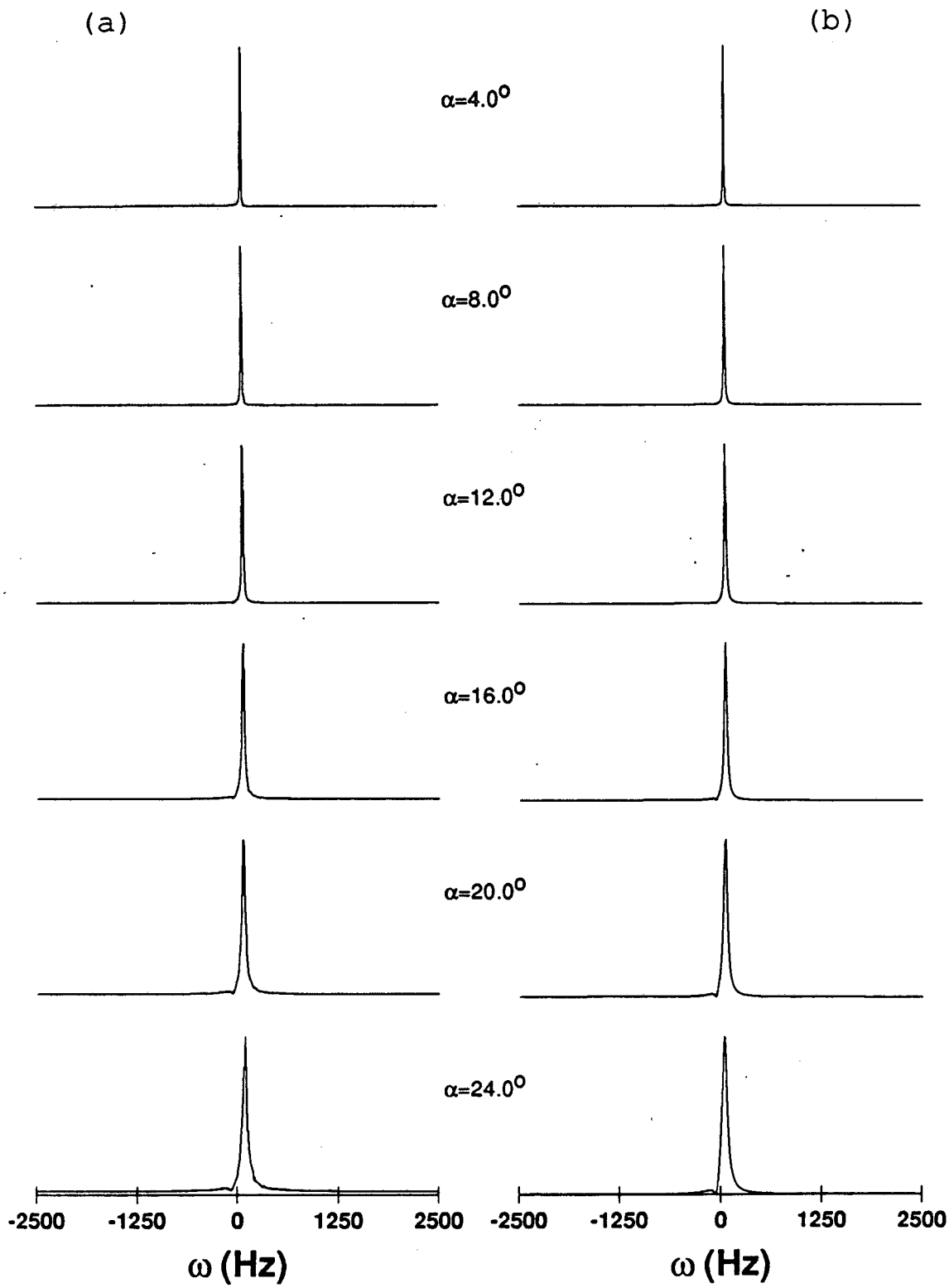
(a)
(b)
α=4.0°
α=8.0°
α=12.0°
α=16.0°
α=20.0°
α=24.0°
-2500
-1250
0
1250
2500
ω (Hz)
-2500
-1250
0
1250
2500
ω (Hz)

LAWRENCE BERKELEY LABORATORY
TECHNICAL INFORMATION DEPARTMENT
UNIVERSITY OF CALIFORNIA
BERKELEY, CALIFORNIA 94720